Biocatalysis and Agricultural Biotechnology 55 (2024) 102972

Contents lists available at ScienceDirect

Biocatalysis and Agricultural Biotechnology

journal homepage: www.elsevier.com/locate/bab

Synthesis and optimization of nanoparticles from *Phragmites karka* improves tomato growth and salinity resilience

Maria Hanif [a], Neelma Munir [a, **], Zainul Abideen [b, *], Jean Wan Hong Yong [c, ***], Ali El-Keblawy [d], Mohamed A. El-Sheikh [e]

[a] *Department of Biotechnology, Lahore College for Women University, Lahore, Pakistan*
[b] *Dr. Muhammad Ajmal Khan Institute of Sustainable Halophyte Utilization, University of Karachi, 75270, Pakistan*
[c] *Department of Biosystems and Technology, Swedish University of Agricultural Sciences, Alnarp, 23456, Sweden*
[d] *Department of Applied Biology, College of Sciences, University of Sharjah, Sharjah, P.O. Box 27272, United Arab Emirates*
[e] *Botany & Microbiology Department, College of Science, King Saud University, P.O. Box 2455, Riyadh, 11451, Saudi Arabia*

ARTICLE INFO

Handling Editor: Dr. Ching Hou

Keywords:
Phragmites karka
Halophytes
Zinc oxide nanoparticles
Salt resilience
Tomato plant
Zeta-potential

ABSTRACT

Halophytes contain many secondary metabolites that can facilitate the capping and stabilizing of nanoparticles. Synthesis and optimization of zinc oxide nanoparticles from *Phragmites karka* were performed for the first time in this study to assess the salinity resilience of tomato seedlings in 100 mM NaCl using biotechnological applications and growth analysis. Response surface methodology and central composite design data revealed that ZnO NPs were stable at a 2:1 ratio of plant and salt concentration (pH of 6.5 at 37.5 °C). The peak obtained at 331 nm from UV–Vis spectroscopy confirmed the synthesis of ZnO NPs and these NPs have multiple functional groups. The chemical bond formation of the prepared ZnO NPs (assessed using FTIR and XRD) confirmed the crystalline structure of ZnO NPs that were derived from halophyte *P. karka*. The SEM images revealed that ZnO NPs have a particle size of 23.5 nm and are spherical, while DLS revealed the size (32.6 nm) and zeta-potential (−6.43 mV) of nanoparticles. Plants treated with ZnO NPs increase the overall tomato growth parameters under salt stress, including shoot length (3-fold), especially at T20 (50 mgL^{-1} ZnO NPs + 100 mM NaCl) treatment among all growth weeks. The number of leaves increased at T16 (20 mgL^{-1} ZnO NPs + 100 mM NaCl). The numbers of nodes and internodes were increased at T20 (50 mgL^{-1} ZnO NPs + 100 mM NaCl) in both parameters. Halophytic nanoparticles could be beneficial sources of biostimulants to improve salt resilience of tomato plants undergoing salt stress.

1. Introduction

Nanoparticles (NPs) are increasingly used in agriculture to boost crop productivity, protect against pests and diseases, and improve nutrient use efficiency. In the 21st century, applying NPs in agriculture increases plant production and stress resilience. For ex-

Abbreviations: ANOVA, Analysis of Variance; C.V, Co-efficient of Variation; CCD, Central Composite Design; DLS, Dynamic Light Scattering; FESEM, Field Emission Scanning Electron Microscopy; FT-IR, Fourier Transform Infrared Spectroscopy; JCPDS, Joint Committee on Powder Diffraction Standards; MFAT, Multiple Factor at a Time; OFAT, One Factor at a Time; RCBD, Randomization Complete Block Design; RSM, Response Surface Methodology; *P. karka*, *Phragmites karka*; XRD, X-ray Diffraction.

* Corresponding author.
** Corresponding author.
*** Corresponding author.
E-mail addresses: neelma.munir@lcwu.edu.pk (N. Munir), zuabideen@uok.edu.pk (Z. Abideen), jean.yong@slu.se (J.W. Hong Yong).

https://doi.org/10.1016/j.bcab.2023.102972
Received 9 October 2023; Received in revised form 17 November 2023; Accepted 27 November 2023
Available online 5 December 2023

ample, NPs are increasingly being utilized as nanofertilizers to deliver nutrients to plants more efficiently than traditional fertilizers. Using chemical fertilizers enhances the possibility of harming living organisms and hinders the ecological and environmental safety of the ecosystem (Shang et al., 2019). In addition, NPs can be used to encapsulate pesticides, which allows for a controlled release of the active ingredient (Huang et al., 2018). Therefore, using NPs in agriculture reduces the amount of chemicals necessary, minimizes environmental contamination, and increases fertilizer and pesticide efficacy.

In nano-industry, ZnO NPs are abundantly used as their manufacturing rate is higher than other NPs. The extensive use of synthetic nanoparticles may accumulate in the ecosystem and could be transferred to the food chain as they have the potential to absorb and accumulate pollutants (Al-Jabri et al., 2022). This pathway may damage the sub-cellular organization and plant photosynthesis (Ali et al., 2021). The green synthesis of NPs is an environmentally friendly and cost-effective method as it avoids the formation of harmful by-products and reduces environmental pollution (Chan et al., 2022; Bora et al., 2022; Jakhar et al., 2022). The biosynthesis of metal and metal oxide nanoparticles could be done using plant extracts, algae, bacteria, or fungal cellular culture. Among all these sources, the synthesis of plant extract nanoparticles is beneficial due to the accumulation of stress-protective metabolites (Shafey, 2020; Munir et al., 2021). Several extraction techniques have been developed for processing agricultural by-products. Among these, ultrasound-assisted and microwave-assisted extraction could be used to extract secondary metabolites, such as polyphenols, from plant materials (Tao et al., 2022; 2022). The polyphenols from liquid can be extracted using simple and selective methods (Tao et al., 2022).

Zinc is an essential micronutrient for plant yield and development. It also plays a vital role in various plants' physiological processes, such as the synthesis of hormones, plant chlorophyll synthesis, and the development of chloroplast. Zinc is also vital for the development of chloroplasts and for the maintenance and stability of cell membrane structure. The biosynthesis of NPs mainly depends on the biomolecules present in plants, such as enzymes, amino acids, organic acids, vitamins, and proteins. These biomolecules act as capping agents in the production of metal nanoparticles. ZnO NPs are non-toxic, cost-effective, and environmentally friendly, benefiting plant vegetation and maturation. They are recommended to be safe for the food chains compared to other metal nanoparticles (Ying et al., 2022).

The plant yield usually decreases due to the salt stress, a primary abiotic stress. The salt stress might cause the increase of Na^+ and Cl^- ions in plants which decreases yield and increases morpho-physiological disorders. The accumulation of Na^+ and Cl^- ions leads to osmotic stress, ion toxicity, and water reduction in plant tissue (Ma et al., 2020). NPs of suitable size (1–100 nm) can penetrate plants by mineral aggregation in the subcellular part of plants. These halophyte NPs protect plants against multiple abiotic stressors (Kesawat et al., 2023; Munir et al., 2021). Halophytes, such as *Panicum antidotale, Halopyrum mucronatum, Desmostachya bipinnata, Phragmites karka, Chenopodium album,* and *Withania somnifera*, could be a source of nanoparticles and serve as biostimulants to increase salt tolerance in crop plants (Meng et al., 2018). *Phragmites karka* is a rhizomatic perennial reed that can resist up to 400 mM NaCl due to the accumulation of stress-protecting secondary metabolites (Abideen et al., 2014). It cannot be used as fodder but as an excellent stabilizer for eroding river banks (Ansari et al., 2021). The current research deals with the biogenic synthesis of ZnO NPs from the leaves of *P. karka.* Multiple experimental parameters have been optimized for the stable synthesis of ZnO NPs using Design Expert RSM. These parameters are temperature, pH, plant extract and salt solution ratio, and time for NPs synthesis. These biogenically synthesized nanoparticles were characterized using UV–Vis spectrophotometer, FTIR, FESEM, XRD, and DLS. For application purposes, these ZnO NPs were applied on tomato plants under salinity stress for *ex vitro* analysis. The main aim of present project was to synthesize ZnO NPs from halophyte *P. karka* leaves using RSM and to analyze its application on tomato plants under saline stress.

2. Materials and methods

2.1. Materials

The chemicals used in this study consisted of zinc acetate dihydrate $(CH_3{\cdot}COO)_2Zn.2H_2O$, sodium hydroxide (NaOH), hydrochloric acid (HCl), sodium hypochlorite solution (NaOCl) and sodium chloride (NaCl) purchased from Biochem Chemopharma. The equipment used in this study included: a weighing balance, water bath (DAEYANG ETS), pH meter (InoLab), shaking incubator (IRMECO Germany), centrifuge (MPW-260R), dry oven (DAEYANG ETS), muffle furnace (Local made, PCSIR), UV–Vis spectrophotometer (U-2800 Spectrophotometer), SEM (ZEISS LS10), XRD (D8Discover Brooker), FTIR (IRTracer-100 SHIMADZU) and a DLS (Malvern).

2.2. Methods

2.2.1. Sampling of P. karka leaves

Fresh and healthy leaves of *P. karka* were sampled from Karachi, Pakistan, and washed 2–3 times using distilled water to eliminate dust particles on the surface. The washed leaves were shade-dried for at least 1 week at room temperature. The dried leaves were carefully packed in a labeled polythene bag and sealed properly. Then, the sample was parceled to Lahore College for Women University, Lahore, Pakistan (Fig. 1).

2.2.2. Preparation of extract

The dried *P. karka* leaves were then finely grinded into a powder. The finely grounded powder was stored in a labeled airtight jar at room temperature for further research. Five (gm) powdered leaves were weighed and added in a separately labeled conical flask with 100 ml of distilled water to make a homogenous mixture. The labeled flask was kept in a water bath for about 30 min at 60 °C followed by filtration using Whatman filter Paper No.1 and stored in an amber-colored bottle at 4 °C (Hosny et al., 2021).

Fig. 1. Sampling of *P. karka* leaves from Karachi, for the green synthesis of ZnO nanoparticles. (For interpretation of the references to color in this figure legend, the reader is referred to the Web version of this article.)

2.2.3. Biogenic synthesis and purification of ZnO NPs from P. karka leaf extract

ZnO nanoparticles from *P. karka* were synthesized by the method as reported by Faisal et al. (2021) with little modification. To synthesize ZnO NPs, a 2:1 ratio of leaf extract and salt solution was used. A salt solution of 0.25 M Zinc acetate dihydrate (Zn $(CH_3COO)_2.2H_2O$) was prepared. Salt solution was added in leaves extract gradually drop by drop in a 250 ml conical flask under continuous stirring on a magnetic stirrer at 900 rpm for about 2 h until the color changed from light green to pale yellow. The color change of the solution indicated the presence of zinc oxide nanoparticles. pH of the homogenous solution was adjusted to 6.5. This reaction mixture was placed in a shaking incubator at 120 rpm at 37 °C for overnight. ZnO NPs were harvested by centrifuging the reaction mixture at 6000 rpm for 30 min at 25 °C. The supernatant was discarded, and the nano-pellet was washed thrice using distilled water to confirm the removal of other particles. The obtained nano-pellet was dried at 60 °C for about 2 h in a dry oven. The final product was grey powdered NPs, which were mashed using a pestle and mortar. Afterwards, the collected powder was shifted to a ceramic crucible cup. These powdered NPs were calcined in a muffle furnace at 400 °C for 3 h. The resultant grey-colored annealed powder was stored in a labeled Eppendorf for characterization and further research. Fig. 2 shows the diagrammatic presentation of ZnO NPs synthesis.

2.2.4. Statistical optimization of the synthesis parameters for biosynthesized ZnO nanoparticles

The RSM was designed using the Design-Expert 11 software for the optimization parameters used for ZnO NPs synthesis. RSM, which has a central composite design (CCD), was applied. RSM was used to optimize ZnO NPs by *P. karka.* RSM uses statistical-based methodology to analyze the effect of changes in the condition of different variables used for ZnO NPs synthesis to determine the optimum conditions for their synthesis. RSM was applied to analyze the impact of independent variables, i.e., plant extract, salt concentration, pH, and temperature, on the synthesis of ZnO NPs. The CCD was used to estimate the level of four independent variables. A total of 30 runs were carried out to analyze the individual and interactive effects of an independent variable. The absorbance of each factor was considered the dependent response (Y). All four variables were examined at the three coded levels (−1, 0, and +1). This method evaluated the efficiency of three variables simultaneously while keeping the one variable constant. Using the design, the ex-

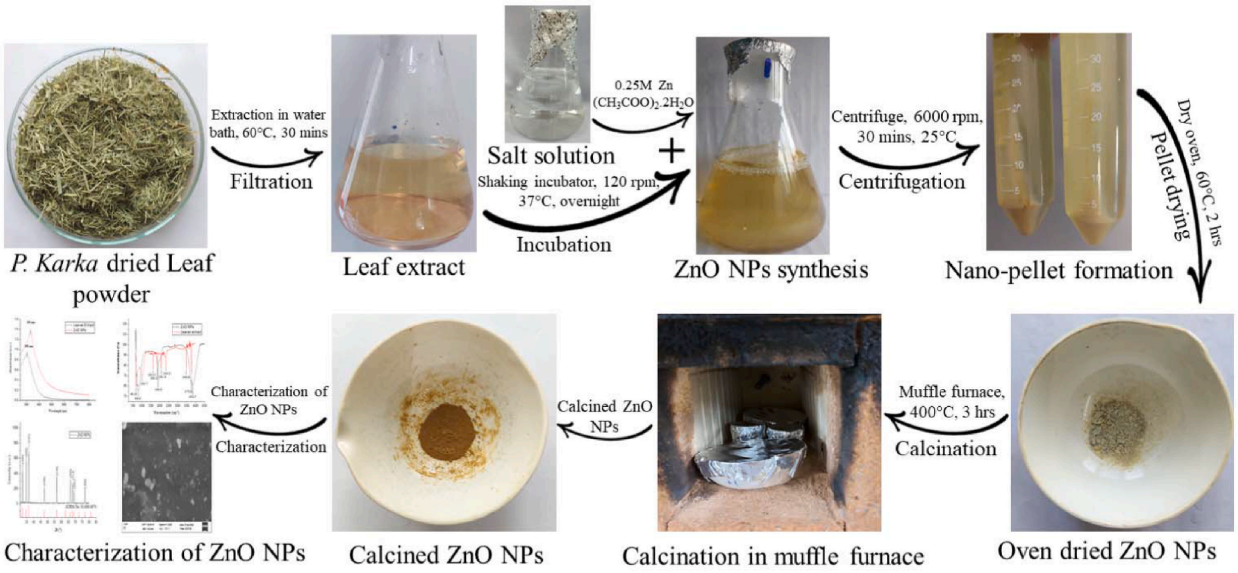

Fig. 2. Diagrammatic presentation of different steps of ZnO NPs synthesis from *Phragmites karka* plants.

perimental data were fitted according to Eq. (1) as a second-order-quadratic equation, including individual and cross-interaction of all variables. The below second-order polynomial equation was used to calculate the interaction between different variables and the response.

$$Y = \beta_0 + \beta_1 X_1 + \beta_2 X_2 + \beta_3 X_3 + \beta_4 X_4 + \beta_{12} X_1 X_2 + \beta_{13} X_1 X_3 + \beta_{14} X_1 X_4 + \beta_{23} X_2 X_3 + \beta_{24} X_2 X_4 + \beta_{34} X_3 X_4 + \beta_{11} X_1^2 + \beta_{22} X_2^2 + \beta_{33} X_3^2 + \beta_{44} X_4^2 \quad \text{(Eq. 1)}$$

Where in Eq. (1), Y is the predicted response, β_0 is the constant term, β_1, β_2, *and* β_3 and β_4 are the regression coefficients for linear effects, β_{12}, β_{13}, β_{14}, β_{23}, β_{24}, and β_{34} denote the regression coefficients for interaction effects, β_{11}, β_{22}, *and* β_{33} and β_{44} refer to the regression coefficients for quadratic effects. The absorbance was measured as the response value Y of the four variables. This software was used to analyze the regression of the experimental data and plot response surface graphs. Multiple coefficients of correlation "R" and determination coefficients of correlation R^2 were calculated for the evaluation of regression equation performance. The fitted polynomial equation was expressed in the form of 3D surface plots. Analysis of Variance (ANOVA) was conducted to specify the significance of the model. The interactive relation between significant variables was analyzed by response surface and contour plots. RSM was used for the regression and graphical analysis of obtained data.

2.2.5. Characterization of synthesized ZnO NPs

The characterization of ZnO nanoparticles synthesized from halophyte (*P. karka*) was carried out using the method reported by Faisal et al. (2021).

2.2.5.1. UV–Vis spectroscopy. The bioreduction of zinc acetate to ZnO NPs was observed periodically by an ultra-violet-visible spectrophotometer (Model: U-2800 Spectrophotometer). UV–Vis analysis of leaf extract and ZnO NPs was carried out, and leaf extract was diluted using distilled water. A UV–Vis spectrograph of leaf extract and ZnO NPs was recorded using a quartz cuvette with water as a reference. The UV–Vis spectrometric readings were measured in the wavelength range 200–800 nm.

2.2.5.2. Fourier Transform infrared spectroscopy. In order to characterize the functional groups present on the surface of synthesized ZnO NPs, the IRTracer-100 Fourier Transform infrared spectrophotometer SHIMADZU was used. The infrared absorption spectrum obtained by this characterization technique identifies the phytochemical agent involved in the capping and stabilization of ZnO NPs. The calcined powder of ZnO NPs was used for the analysis.

2.2.5.3. Field emission scanning electron microscopy. The morphology and size of ZnO nanoparticles were examined by FESEM using SEM ZEISS LS10 with an accelerating voltage between 10 and 20 KV under vacuum conditions. The sample was placed on a carbon-coated copper grid.

2.2.5.4. X-ray diffraction. The crystalline structure and the degree of crystallinity of ZnO NPs were analyzed using an X-ray diffractometer. The scanning range was selected between 10° and 80°.

2.2.5.5. Dynamic light scattering. Zeta-size and zeta-potential were analyzed by DLS on Malvern, Malvern Instruments Limited. The zeta potential values were obtained by applying the Helmholtz-Smoluchowski equation built in Malvern. For analysis, 10 mg of ZnO NPs was dissolved in distilled water and sonicated for 30 min.

2.2.6. Preparation of ZnO NPs suspension

The nanoparticles synthesized from *P. karka* have 32.6 nm particle size and −6.43 mV Zeta potential. For the preparation of multiple nanoparticle concentrations for the *ex vitro* experiment, 1g of synthesized ZnO NPs were dissolved in 1L of distilled water to make a homogenous suspension. The bulk solution of NPs was homogenized using a digital ultrasonic bath for about 30 min at 25 °C with a sonication intensity of 150 W, 40 kHz to achieve a better dispersion of nanoparticles (Alharby et al., 2017).

2.2.7. Tomato plant material and experimental design

This experiment involved developing a tomato (*Solanum lycopersicum* L.) under salt stress by the foliar application of ZnO NPs. The seeds of the tomato were procured from Punjab Seed Corporation, Lahore. The experiment was conducted in Lahore College for Women University, Lahore, in Randomization Complete Block Design (RCBD) under an ex-vitro environmental conditions. Healthy and uniform-size tomato seeds were washed with distilled water and then surface sterilized with 3% sodium hypochlorite solution (NaOCl) for 10 min, followed by repeated washing with sterilized distilled water. The sterilized seeds were sown in a plastic tray (28 × 40 × 16 cm) filled with an equal amount of soil mixed with peat moss and perlite (1:1). At 20 days after sowing (DAS), uniform and healthy tomato seedlings were transplanted to 96 experimental plastic pots (10 cm in diameter and 12 cm in length) for further research purposes. The 96 pots were divided into 24 sets of 4 pots each (replicates) representing one treatment. Tomato plants were irrigated daily with tap water until the harvesting of plants.

The foliar application of ZnO NPs on tomato plants under salt (NaCl) stress was carried out by using four different concentrations of ZnO NPs (10, 20, 50, and 100 mgL^{-1}) and 10, 20, 50, and 100 mM NaCl were applied along with the combination treatments. A total of 24 treatments were carried out, with 4 replicates of each treatment. Consequently, all treatments of ZnO NPs and NaCl salt were applied to each pot in 10-day intervals, starting from 3 weeks old tomato plants until the fruiting stage. To prevent osmotic shock, salinity treatments were gradually applied by the irrigation system when the plants were 3 weeks old (Abideen et al., 2014). Salinity levels were obtained by adding an appropriate amount (20 ml) of NaCl via the irrigation system. The first foliar application of ZnO NPs was carried out with a hand sprayer at 3-week-old plants. At the time of the NPs' spray, the soil surface in pots was covered with a

plastic sheet to avoid direct entry of ZnO NPs in the soil. The tomato crop was grown for about 4 months until the fruiting stage. Table 1 presents the treatments given to the tomato plants in this study.

2.2.8. Analysis of plant morphological parameters

The plants were harvested at 4, 8, 12, and 16 weeks, and growth parameters (e.g., shoot length, number of leaves, number of nodes, and internodes) were measured to assess tomato plants' performance.

2.2.9. Statistical analysis

Data was statistically analyzed using IBM SPSS statistics 25. Standard error was calculated along with the analysis of variance (*ANOVA*) to determine the least significant difference (LSD) between treatment means with the significance level at $p \leq 0.05$.

3. Results

3.1. Statistical optimization of ZnO NPs synthesis by response surface methodology

In this research work, RSM was coupled with CCD to analyze the optimum conditions required for synthesizing stable ZnO NPs using *P. karka*. CCD is a two-level factorial design having center points, i.e., axial or star points. Based on factorial experimental results, four independent variables were selected, i.e., plant (g), salt (g), pH, and temperature (°C) in RSM model. These independent variables were used to analyze their significant effect on absorbance (a.u.) at a specific wavelength. These RSM models were used to compute the precise structure of the model and to study the impact of individual factors. The quadratic model was used to investigate the mathematical relationship between independent and dependent variables. Table 2 represents the experimental ranges and levels of independent variables.

The five coded levels were selected, and four variables were used to design an experimental setup of 30 runs. These runs were analyzed based on the interaction of the individual, quadratic, and cross-products of the variables. The order of the experimental run was arranged randomly. Table 3 shows the experimental design and response activity of ZnO NPs synthesized from *P. karka.*

Table 1
Applied nanoparticle and saline treatments to tomato plants for growth trials.

Treatments	ZnO NPs (mgL^{-1})	NaCl (mM)	ZnO NPs (mgL^{-1}) + NaCl (mM)
T0	Control		
T1	10		
T2	20	_	_
T3	50	_	_
T4	100	_	_
T5	_	10	_
T6	_	20	_
T7	_	50	_
T8	_	100	_
T9	_	_	10 ZnO NPs + 10 NaCl
T10	_	_	10 ZnO NPs + 20 NaCl
T11	_	_	10 ZnO NPs + 50 NaCl
T12	_	_	10 ZnO NPs + 100 NaCl
T13	_	_	20 ZnO NPs + 10 NaCl
T14	_	_	20 ZnO NPs + 20 NaCl
T15	_	_	20 ZnO NPs + 50 NaCl
T16	_	_	20 ZnO NPs + 100 NaCl
T17	_	_	50 ZnO NPs + 10 NaCl
T18	_	_	50 ZnO NPs + 20 NaCl
T19	_	_	50 ZnO NPs + 50 NaCl
T20	_	_	50 ZnO NPs + 100 NaCl
T21	_	_	100 ZnO NPs + 10 NaCl
T22	_	_	100 ZnO NPs + 20 NaCl
T23	_	_	100 ZnO NPs + 50 NaCl
T24	_	_	100 ZnO NPs + 100 NaCl

Table 2
Levels of four factors used in CCD for ZnO NPs synthesis.

Name	Units	Type	Std. Dev.	Low	High
Plant	g	Factor	0	0.5	1.5
Salt	g	Factor	0	0.5	1.5
pH		Factor	0	6	7
Temperature	°C	Factor	0	35	40
Absorbance	a.u.	Response	0.0517998	0.511	0.699

Table 3
Experimental design by CCD and response activity of ZnO NPs from *P. karka*.

Std.	Run	Factor 1 A: Plant powder (g)	Factor 2 B: Salt (g)	Factor 3 C: pH	Factor 4 D: Temperature (°C)	Response 1 Absorbance (a.u.)
29	1	3.5	1	6.5	37.5	0.627
15	2	2	1.5	7	40	0.576
21	3	3.5	1	5.5	37.5	0.573
9	4	2	0.5	6	40	0.599
13	5	2	0.5	7	40	0.617
23	6	3.5	1	6.5	32.5	0.614
3	7	2	1.5	6	35	0.516
19	8	3.5	0	6.5	37.5	0.633
10	9	5	0.5	6	40	0.535
17	10	0.5	1	6.5	37.5	0.627
27	11	3.5	1	6.5	37.5	0.683
2	12	5	0.5	6	35	0.613
18	13	6.5	1	6.5	37.5	0.523
14	14	5	0.5	7	40	0.546
28	15	3.5	1	6.5	37.5	0.602
6	16	5	0.5	7	35	0.567
7	17	2	1.5	7	35	0.645
16	18	5	1.5	7	40	0.545
8	19	5	1.5	7	35	0.677
4	20	5	1.5	6	35	0.52
25	21	5	1	6.5	37.5	0.699
1	22	2	0.5	6	35	0.672
12	23	5	1.5	6	40	0.511
22	24	3.5	1	7.5	37.5	0.681
20	25	3.5	2	6.5	37.5	0.675
11	26	2	1.5	6	40	0.54
30	27	3.5	1	6.5	37.5	0.63
26	28	3.5	1	6.5	37.5	0.646
24	29	3.5	1	6.5	42.5	0.544
5	30	2	0.5	7	35	0.577

3.1.1. Analysis of variance (ANOVA) for quadratic model

ANOVA test is used to analyze the significance and fitness of the model as well as to identify the model lack of fit. The ANOVA analysis represented a linear relationship between the significant effects of independent variables such as plant (g), salt (g), pH, and temperature (°C). ANOVA is a statistical technique used to analyze the relationship of quantitative variables. These quantitative variables can be described as a function of one or more qualitative variables. The main purpose of ANOVA is to observe the significant combination among explanatory variables. This test also analyzes the reliability of the model as a whole. Various models, likewise the linear, 2FI, quadratic, and cubic, were tested to enhance the synthesis of nanoparticles based on their F-value, *p*-value, determination co-efficient (R^2), and standard deviation. Table 4 shows the ANOVA for the quadratic model of *P. karka*.

Table 4
ANOVA for Quadratic model of *P. karka* ZnO NPs.

Source	Sum of Squares	df	Mean Square	F-value	p-value	
Model	0.0696	14	0.0050	2.90	0.0248	significant
A-Plant	0.0079	1	0.0079	4.62	0.0484	
B-Salt	0.0005	1	0.0005	0.3045	0.5892	
C-pH	0.0088	1	0.0088	5.14	0.0386	
D-Temperature	0.0087	1	0.0087	5.09	0.0394	
AB	0.0020	1	0.0020	1.18	0.2945	
AC	0.0003	1	0.0003	0.1684	0.6873	
AD	0.0016	1	0.0016	0.9557	0.3438	
BC	0.0137	1	0.0137	7.98	0.0128	
BD	0.0002	1	0.0002	0.1062	0.7490	
CD	0.0001	1	0.0001	0.0771	0.7851	
A^2	0.0148	1	0.0148	8.64	0.0102	
B^2	0.0003	1	0.0003	0.1958	0.6645	
C^2	0.0029	1	0.0029	1.68	0.2146	
D^2	0.0136	1	0.0136	7.91	0.0131	
Residual	0.0257	15	0.0017			
Lack of Fit	0.0190	10	0.0019	1.42	0.3673	not significant
Pure Error	0.0067	5	0.0013			
Cor Total	0.0954	29				

In Table 4, P-value of the model was 0.0248, which is less than 0.05; thus, this quadratic model is significant. It has been observed that in Table 4, temperature (Factor 4) has attained the highest F-value, *i.e.,* 7.91 the highest F-value of a temperature indicates that the temperature plays a major role in the absorbance of nanoparticles synthesized from *P. karka.*

In Table 4, the Model F-value of 2.90 indicates that the model is significant. There is only a 2.48% chance that a higher F-value could occur due to noise. The model F-value was the result of the variance analysis between the established model and residues. The significance of each coefficient can be determined by observing the F-value and *p*-value. In Table 4, P-values less than 0.0500 indicate model terms are significant. In this case A, C, D, BC, A^2, D^2 are significant model terms. Values greater than 0.1000 indicate the model terms are not significant. The estimated *p*-value showed that only plant (g), pH, and temperature (°C) significantly affected the synthesis of ZnO NPs from *P. karka.*

According to Table 4 of ANOVA, the Lack of Fit F-value of 1.42 implies the Lack of Fit is insignificant relative to the pure error. There is a 36.73% chance that a Lack of Fit F-value this large could occur due to noise.

3.1.2. Fit statistics

The coefficient of variation (C.V.) identifies the reliability of the statistical model. It is the ratio of the estimated standard error to the mean value of the observed response. Table 5 indicates the ANOVA summary of fit statistics. The C.V. value of less than 10% is desirable.

Table 5 indicates that the Predicted R^2 of 0.2509 is in reasonable agreement with the Adjusted R^2 of 0.4781; *i.e.,* the difference is less than 0.2. Adequate Precision measures the signal-to-noise ratio. A ratio greater than 4 is desirable. The ratio of 5.820 indicates an adequate signal. This model can be used to navigate the design space. The C.V. value is less than 10% i.e. 6.90%, which means this model is also highly significant.

3.1.3. Final equation in terms of coded factors

The final equation in terms of coded factors for absorbance by *P. karka* ZnO NPs is presented below:

$$\text{Absorbance} = +\ 0.6478 - 0.0182*A - 0.0047*B + 0.0192*C - 0.0191*D + 0.0113*AB + 0.0043*AC - 0.0101*AD + 0.0293*BC - 0.0034*BD - 0.0029*CD - 0.0232*A^2 - 0.0035*B^2 - 0.0102*C^2 - 0.0222*D^2 \quad \text{(Eq. 2)}$$

In Eq. 2, A represents plant sample (g), B represents salt (g), C is coded for pH, and D indicates temperature. The coded factors equation can be used to predict the response for given levels of each factor. By default, the high levels of the factors are coded as +1, and the low levels are coded as −1. The coded equation is useful for identifying the relative impact of the factors by comparing the factor coefficients.

3.1.4. Final equation in terms of actual factors

The final equation in terms of actual factors for absorbance by *P. karka* ZnO NPs is presented below:

$$\text{Absorbance} = -\ 6.21678 + 0.109639*\text{Plant} - 0.693083*\text{Salt} + 0.520750*\text{pH} + 0.286467*\text{Temperature} + 0.015000*\text{Plant}*\text{Salt} + 0.005667*\text{Plant}*\text{pH} - 0.002700*\text{Plant}*\text{Temperature} + 0.117000*\text{Salt}*\text{pH} - 0.002700*\text{Salt}*\text{Temperature} - 0.002300*\text{pH}*\text{Temperature} - 0.010333*\text{Plant}^2 - 0.014000*\text{Salt}^2 - 0.041000*\text{pH}^2 - 0.003560*\text{Temperature}^2 \quad \text{(Eq. 3)}$$

The equation in terms of actual factors can be used to predict the response for given levels of each factor. Here, the levels should be specified in the original units for each factor. Eq. (3) should not be used to determine the relative impact of each factor because the coefficients are scaled to accommodate the units of each factor, and the intercept is not at the center of the design space.

3.1.5. Residual plots

The residual plots usually depict the adequacy of the model. The residual plots assist in evaluating the reliability of the model. These plots help identify the differences between the experimentally derived and predicted values. The normal probability plot is used to analyze the normality of residuals. To analyze experimental data, it is necessary to confirm whether the data have a normal distribution. In normal distribution, the data points follow a straight line and are close to each other. Fig. 3 depicts the normal probability plot of ZnO NPs absorbance from *P. karka.* Fig. 3 illustrates that the points are near the diagonal line, indicating low discrepancies. The straight line in the normal probability plot tells us that the distribution is normal.

Fig. 4 illustrates the relationship between the predicted vs actual absorbance values of ZnO NPs synthesized from *P. karka.* It was estimated from the plot that the quadratic model was significant for the analysis of response variables and input variables. The linear correlation coefficients in plot indicates that there is a reasonable agreement between the independent variables and absorbance values. The results indicate that there are tendencies in the linear regression fit, which proves strong agreement of the ac-

Table 5
Summary of ANOVA fit Statistics by *P. karka.*

Std. Dev.	0.0414	R^2	0.7300
Mean	0.6004	Adjusted R^2	0.4781
C.V. %	6.90	Predicted R^2	0.2509
		Adequate Precision	0.3204

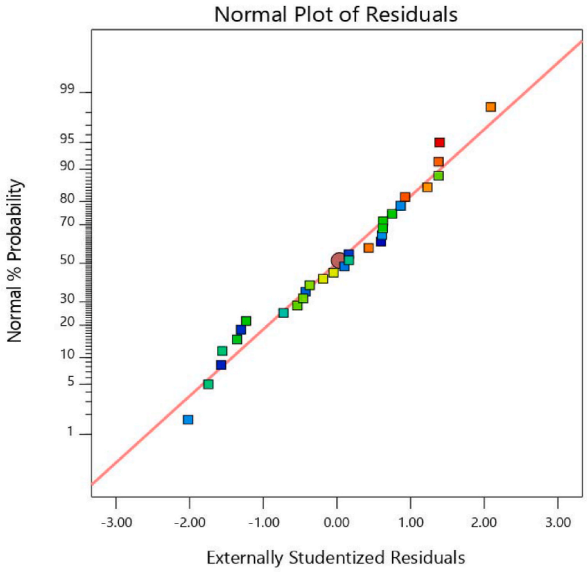

Fig. 3. Normal probability plot for the synthesized nanoparticles absorbance for *P. karka.*

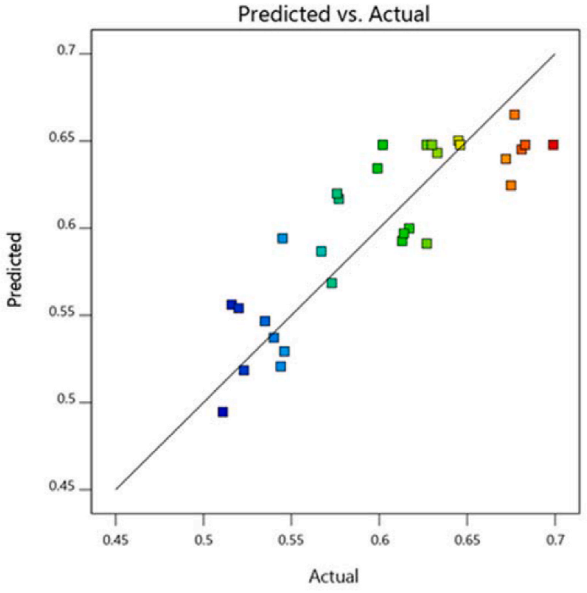

Fig. 4. Predicted vs actual plot of residuals for *P. karka* ZnO NPs.

tual values with the predicted value. The figure can estimate that data points are uniform and consistent along the straight line, which depicts data having a high correlation.

Fig. 5 shows the residual vs. run plot for ZnO NPs absorbance from *P. karka.* The threshold value of ±3.87 standard deviations in the plot was chosen. Any observation outside this threshold points out the potential error in the model. Fig. 5 demonstrates that no data point was outside the threshold value of ±3.87, thus, all models strongly agree with the experimental data. This plot was used to analyze the outliers' values in the data.

3.1.6. Response surface plot analysis

Fig. 6 shows the contour plot for the absorbance of ZnO NPs synthesized from *P. karka,* while Fig. 7 shows the 3D surface plot for the absorbance of ZnO NPs synthesized from *P. karka.* These plots illustrate the interaction effects of independent variables on response. The main purpose of nanoparticle synthesis optimization is to analyze all independent factor values that may lead to the desired response, i.e., absorbance. The contour graphs are used to optimize multiple variables and to identify significant parameters. The contour graph allows the visual drawing and locating of the experimental field area with maximum response. These contour graphs also help to recognize significant interactions between various factors that can lead to the desired response. The quadratic re-

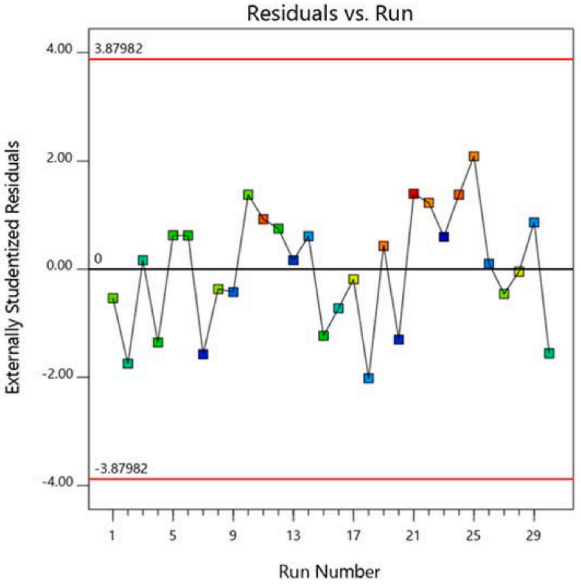

Fig. 5. Residual vs Run plot of residuals for *P. karka* ZnO NPs.

sponse surface model can be analyzed using a 3D response surface and two-dimensional contour plots. One variable was held constant in these plots, and the other two were used within experimental ranges. Fig. 6 shows the contour plots for RSM quadratic models. Besides, Fig. 6b shows the plot against the plant (g) and salt (g) variables for the absorbance of ZnO NPs. This plot illustrates that increasing plant and salt concentration leads to a reduction in the absorbance value.

In the case of *P. karka*, the concentration of plants plays a significant function in the synthesis of ZnO NPs. Fig. 6b, d, and f illustrate that the lower concentration of plants causes the increase of absorbance. Thus, the plant concentration has a significant interaction with the NPs absorbance. Figs. 6h and 4l shows that the increase in salt causes an increase in absorbance. In addition, Fig. 6j predicts that lower temperature causes an increase in absorbance. Thus, it can conclude that all of these variables, i.e., plant (g), salt (g), pH, and temperature (°C) have significant effects on the absorbance of ZnO NPs synthesized from *P. karka.*

3.2. Characterization of synthesized ZnO nanoparticles

The ZnO NPs were synthesized from the leaves extract of halophyte, i.e., *P. karka.* The leaf extract was used due to excess polyphenol content, a vital constituent for the synthesis of ZnO NPs. The presence of phytochemicals in the leaves extract, such as polyphenols, terpenoids, tannins, anthocyanins, and steroids, acts as capping agents in the synthesis of ZnO NPs. The successful synthesis of ZnO NPs by *P. karka* was observed by the change in the color of the reaction mixture from light green to pale yellow. The change in color is considered to be a preliminary indication for the synthesis of ZnO NPs.

3.2.1. UV–visible spectroscopy

The UV–Vis spectrophotometry analysis further confirmed the synthesis of ZnO NPs. The sample spectra recording was performed at a 200–800 nm wavelength range. The ZnO NPs show a characteristic broad absorption peak between 300 and 400 nm. Fig. 8 illustrates the ZnO NPs' UV–Vis spectrum compared with the leaves extract of *P. karka.* The spectrum showed a peak at 331 nm which is diagnostic for the presence of ZnO NPs. Leaves extract showed the highest absorption peak at 302 nm. The obtained data was graphically plotted and represented using the "OriginPro 2018".

3.2.2. Fourier transform infrared spectroscopy (FTIR)

FTIR is used as a confirmatory technique for characterizing synthesized ZnO NPs. This technique helps to identify the vibrational as well as rotational modes of existing molecules. This technique aids in recognizing the functional phytobio-molecules that help in the reduction and stabilization of ZnO NPs. The FTIR spectra of leaf extract and biosynthesized ZnO NPs were recorded in the absorption band 4500 cm^{-1} to 500 cm^{-1}. Fig. 9 illustrates the graphical presentation of FTIR spectra designed from the ZnO NPs synthesized from the leaves extract of *P. karka.* The black-colored spectra illustrate ZnO NPs having multiple peaks, i.e., 698.45 cm^{-1}, 1896.02 cm^{-1}, and 3832.57 cm^{1}. While in the case of *P. karka* leaves extract, the red-colored spectra showed multiple peaks at 661.58 cm^{-1}, 1008.77 cm^{-1}, 1622.13 cm^{-1}, 1863.23 cm^{-1}, 2081.19 cm^{-1}, 2343.51 cm^{-1}, 3469.93 cm^{-1} and 3770.83 cm^{-1}. The peak observed at 661.58 cm^{-1} represents the presence of weak band C–Cl vibration of alkyl halides in leaves extract of *P. karka.* This peak is shifted to 698.45 cm^{-1} in the spectra of NPs which corresponds to the presence of the Zn–O bond. Thus, results showed that ZnO NPs have been synthesized using the leaf extract of *P. karka.* The peaks at 1896.02 cm^{-1} and 1863.23 cm^{-1} were due to the presence of the aldehyde (CHO) group. Peaks ranging from 3832.57 cm^{-1} to 3770.83 cm^{-1} dictate the presence of OH stretching vibrations.

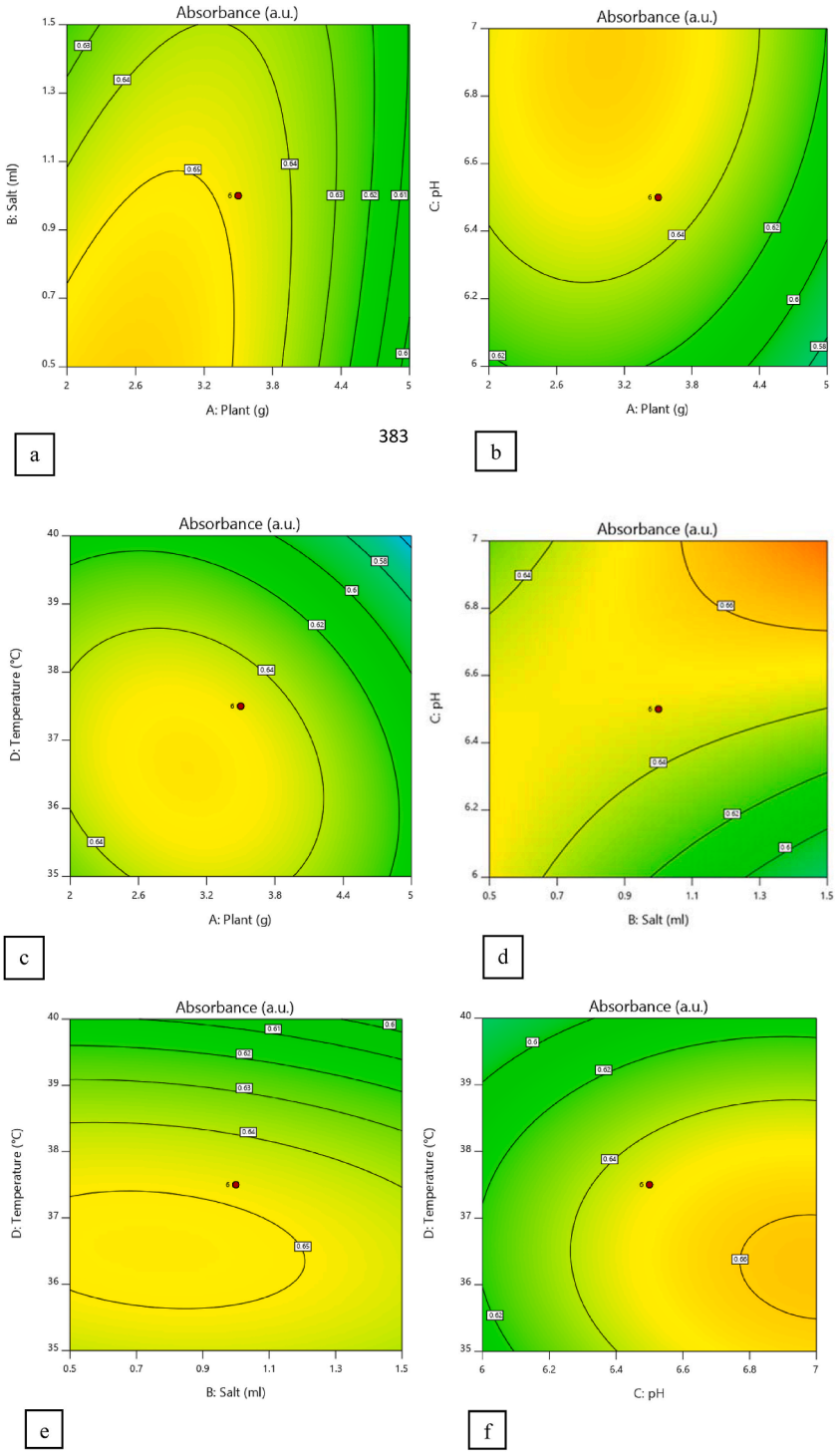

Fig. 6. Graphical representation for response surface optimization by plotting absorbance versus (a) contour plot for plant (g) and salt (g) by *P. karka* ZnO NPs (b) contour plot for plant (g) and pH by *P. karka* ZnO NPs (c) contour plot for plant (g) and temperature (°C) by *P. karka* ZnO NPs (d) contour plot for salt (g) and pH by *P. karka* ZnO NPs (e) contour plot for salt (g) and temperature (°C) by *P. karka* ZnO NPs (f) contour plot for pH and temperature (°C) by *P. karka* ZnO NPs.

3.2.3. X-ray diffraction analysis (XRD)

The XRD pattern of biosynthesized ZnO NPs from *P. karka* leaves extract has been represented in Fig. 10. The XRD pattern showed the noticeable peaks corresponding to 2θ values of 31.8°, 34.5°, 36.3°, 47.6°, 56.6°, 66.4°, 67.9°, 69.08° and 76.9°. These prominent peaks were corresponding to the HKL values of (100), (002), (101), (102), (110), (200), (112), (201) and (202). These planes closely

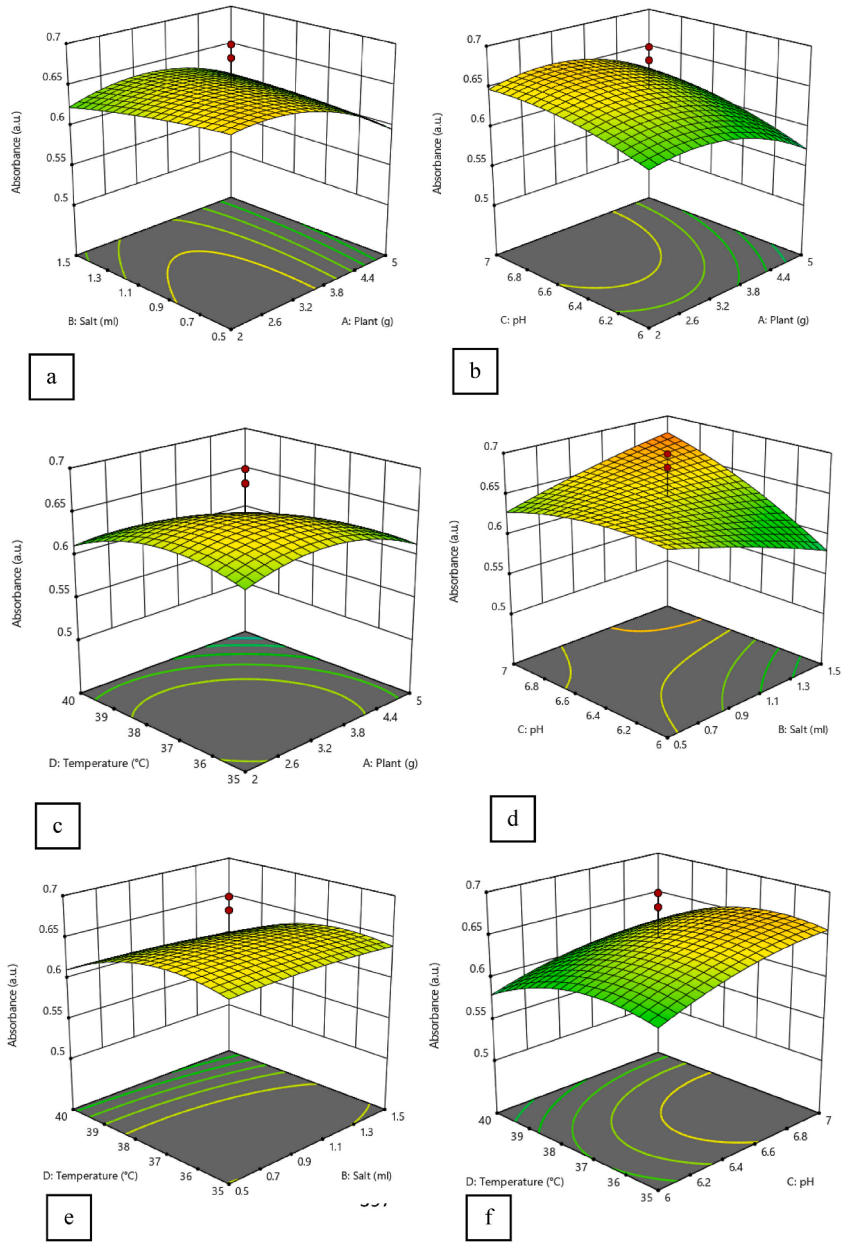

Fig. 7. Graphical representation for response surface optimization by plotting absorbance versus (a) 3D plot for plant (g) and salt (g) by *P. karka* ZnO NPs (b) 3D plot for plant (g) and pH by *P. karka* ZnO NPs (c) 3D plot for plant (g) and temperature (°C) by *P. karka* ZnO NPs (d) 3D plot for salt (g) and pH by *P. karka* ZnO NPs (e) 3D plot for salt (g) and temperature (°C) by *P. karka* ZnO NPs (f) 3D plot for pH and temperature (°C) by *P. karka* ZnO NPs.

matched the crystalline structure of ZnO NPs. These results were also compared with the standard XRD pattern of ZnO NPs with code Joint Committee on Powder Diffraction Standards (JCPDS) card No. 01-080-0074.

3.2.4. FESEM analysis

Fig. 11a and bshows the SEM images for ZnO NPs synthesized from *P. karka.* The images were recorded at the magnification of 5.00 KX and 10.00 KX. SEM images showed that particles are uniformly shaped and spherical. A fairly large number of small molecules and agglomerated particles confirm the synthesis of ZnO NPs. The size of ZnO NPs synthesized from *P. karka* was 23.5 nm.

3.2.5. Dynamic light scattering (DLS)

The Zeta potential of ZnO NPs helps to analyze the stability of synthesized nanoparticles as it gives the net electrostatic potential of any particle in suspension. Fig. 12a shows the zeta potential of ZnO NPs synthesized from *P.* karka. Further, Fig. 12b shows the zeta-size analysis of ZnO NPs synthesized from *P.* karka. The intensity of light scattered due to the movement of nanoparticles was

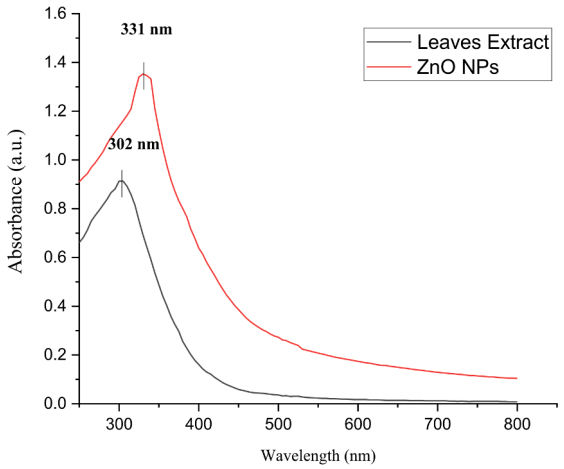

Fig. 8. UV–Vis spectrum of synthesized ZnO NPs compared with leaf extract of *P. karka.*

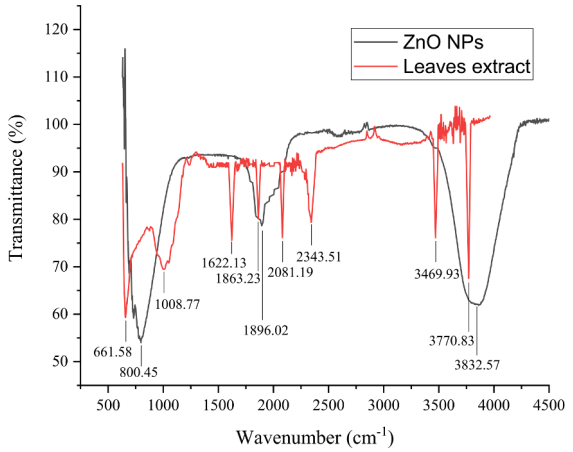

Fig. 9. The overlay of FTIR spectra of leaf extract of *P. karka* compared with biosynthesized ZnO NPs.

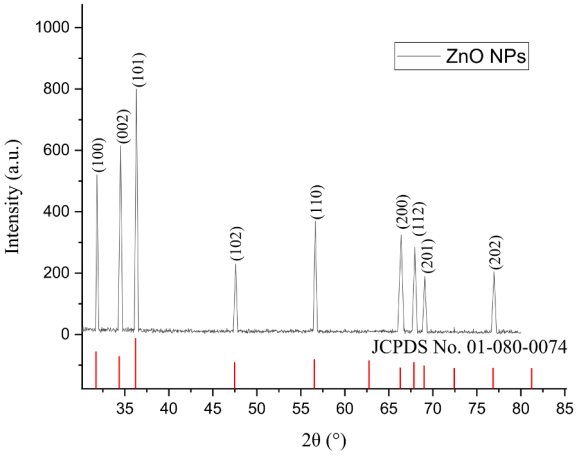

Fig. 10. XRD pattern of synthesized ZnO NPs using *P. karka* leaves extract.

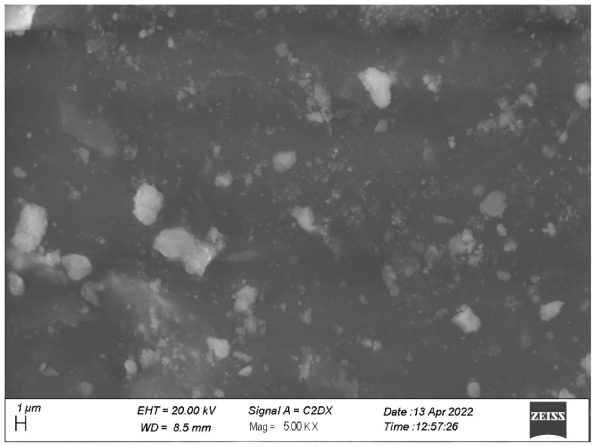

Fig. 11a. The FESEM images of ZnO NPs at magnification of 5.00 KX.

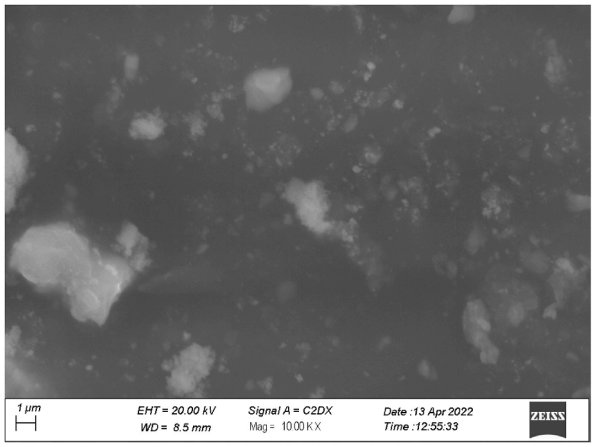

Fig. 11b. The FESEM images of ZnO NPs at a magnification of 10.00 KX.

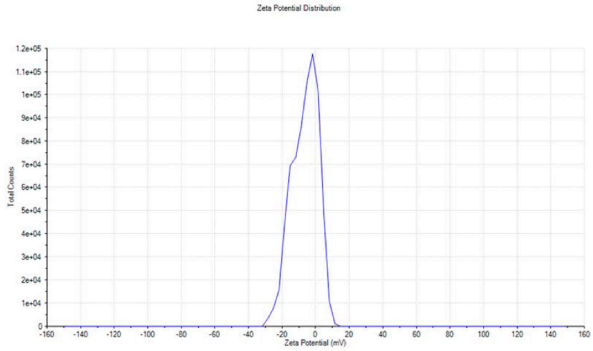

Fig. 12a. Zeta-potential analysis for ZnO NPs synthesized by *P. karka* leaves extract.

measured using a Zeta-sizer. The average size of ZnO NPs synthesized from *P. karka* is 32.6 nm with a polydispersity index (PDI) of 0.608 and −6.43 mV zeta potential.

3.3. Effect of foliar application of ZnO NPs on tomato growth under salinity stress

3.3.1. Shoot length

Figs. 13 and 14 showed the effect of ZnO NPs on tomato plants under salinity stress for various weeks. Results showed the significant increase in shoot length at T3 (50 mgL^{-1} ZnO NPs) treatment of ZnO NPs compared to control. The shoot length increases at the optimum dose of ZnO NPs, but at higher dose the shoot length gradually starts decreasing among all the growth weeks. How-

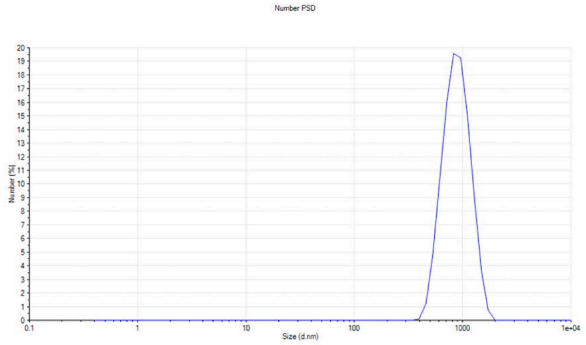

Fig. 12b. Zeta-size analysis for ZnO NPs synthesized by *P. karka* leaves extract.

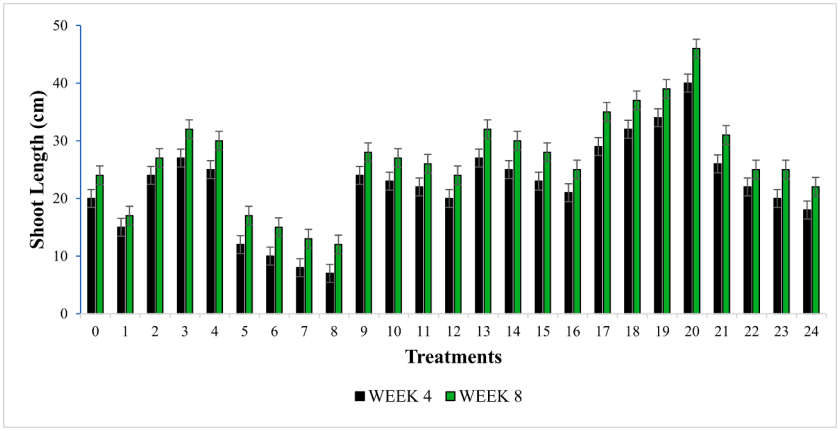

Fig. 13. Week 4th and 8th shoot length of tomato plants subjected to ZnO NPs and salt stress.

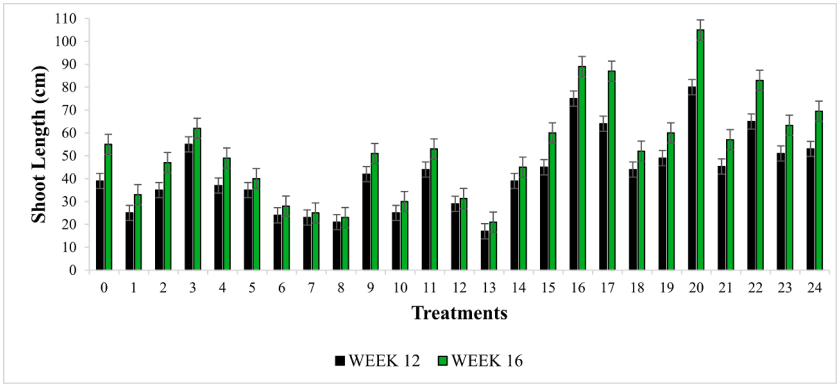

Fig. 14. Week 12th and 16th shoot length of tomato plants subjected to ZnO NPs and salt stress.

ever, under salinity stress, a significant decrease was observed in T5 (10 mM NaCl), T6 (20 mM NaCl), T7 (50 mM NaCl), and T8 (100 mM NaCl) treatments as the concentration of salinity levels increased in comparison with the control. Among all the other comparison treatments, where tomato plants were grown under salinity stress by the foliar application of ZnO NPs, T20 (50 mgL^{-1} ZnO NPs + 100 mM NaCl) showed a significant increase in shoot length.

3.3.2. Number of leaves

Results for the number of leaves showed distinct responses at ZnO NPs and salt stress treatments individually among all growth weeks (Figs. 15 and 16). In the case of nanoparticle treatments, the number of leaves increases with the increase in the nanoparticle dose, but at higher concentrations of nanoparticle treatment T4 (100 mgL^{-1}), the number of leaves gradually decreases. Thus, it can be concluded that T3 (50 mgL^{-1}) showed highest number of leaves. All the treatments only under salt stress showed significant decrease in leaves number in response to 10 mM NaCl, 20 mM NaCl, 50 mM NaCl and 100 mM NaCl as compared to control tomato

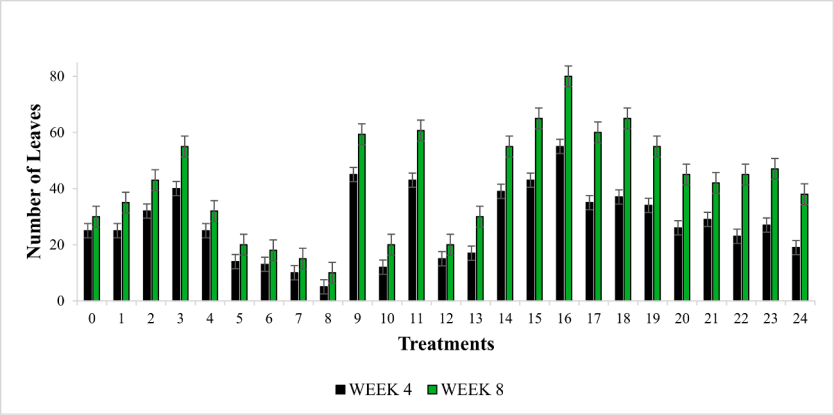

Fig. 15. Week 4th and 8th number of leaves of tomato plants subjected to ZnO NPs and salt stress.

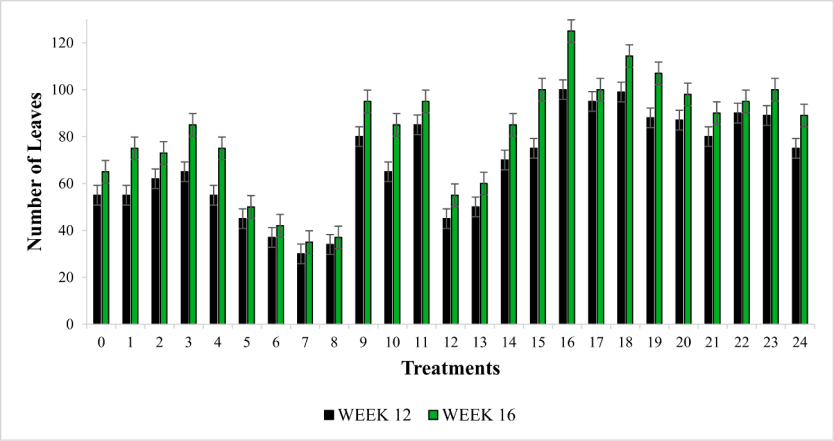

Fig. 16. Week 12th and 16th leaf numbers of tomato plants subjected to ZnO NPs and salt stress.

plants. When tomato plants were treated with the comparison treatments, the highest number of leaves was observed at T16 (20 mgL^{-1} ZnO NPs + 100 mM NaCl).

3.3.3. Number of nodes

Compared with the control sample, the number of nodes gradually increases as the concentration of nanoparticle increases until the concentration reaches at 100 mgL^{-1} ZnO NPs in weeks 12 and 16. Thus, it can be concluded that T3 showed a significant increase in number of nodes. Compared with the control and salinity level, the number of nodes decreased as the salinity concentration increased at all growth weeks. Foliar spray of ZnO NPs at tomato plant under salinity stress causes a noticeable increase in number of nodes only at T14 (20 mgL^{-1} ZnO NPs + 20 mM NaCl) and T20 (50 mgL^{-1} ZnO NPs + 100 mM NaCl) treatments (Figs. 17 and 18).

3.3.4. Number of internodes

Figs. 19 and 20 show the response of salt stress and nanoparticle treatments to the number of internodes in tomato plants. Treatments having only foliar spray of ZnO NPs showed an increase in the number of internodes at an optimum concentration of ZnO NPs at T3 (50 mgL^{-1} ZnO NPs). Then, it gradually decreased as the concentration of ZnO NPs increases. On the other hand, the salt-stressed tomato plants showed a significantly decreased in number of internodes than the control plants. Plants with both treatments showed that the number of internodes increased at T20 (50 mgL-1 ZnO NPs + 100 mM NaCl), which is higher than in all the other treatments.

Fig. 21 shows the ex vitro experimental setup of tomato plants subjected to ZnO NPs and salt stress. Fig. 22 shows the morphological traits (shoot length, number of leaves, number of nodes and internodes) of tomato plants subjected to ZnO NPs under salt stress.

4. Discussion

Phytochemicals found in plants are considered stress-protective compounds and could significantly improve salinity stress resistance (Qasim et al., 2017). *Phragmites karka* have the potential to accumulate metal ions as active phytochemicals and could act as bio-reductants and stabilizers for the green synthesis of ZnO NPs. The reduction of Zn acetate to ZnO NPs occurs due to the excitation of surface plasmon vibrations of synthesized nanoparticles. The biosynthesis of ZnO NPs using *P. karka* is regulated by factors such as

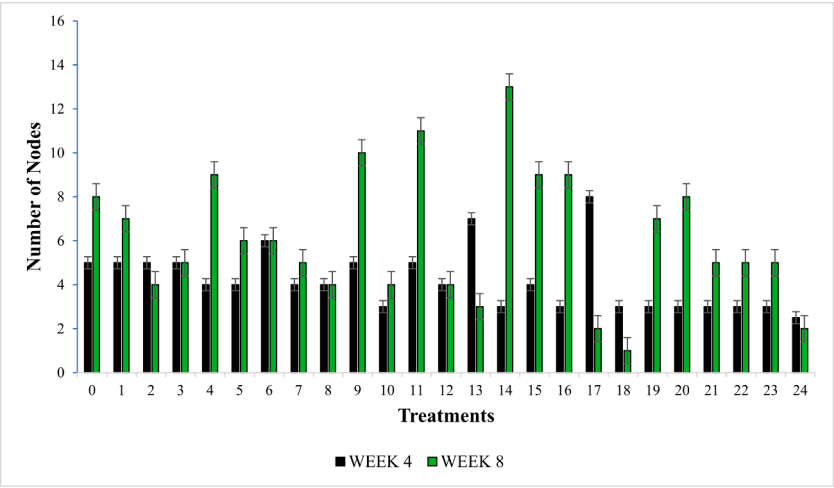

Fig. 17. Week 4th and 8th number of nodes of tomato plants subjected to ZnO NPs and salt stress.

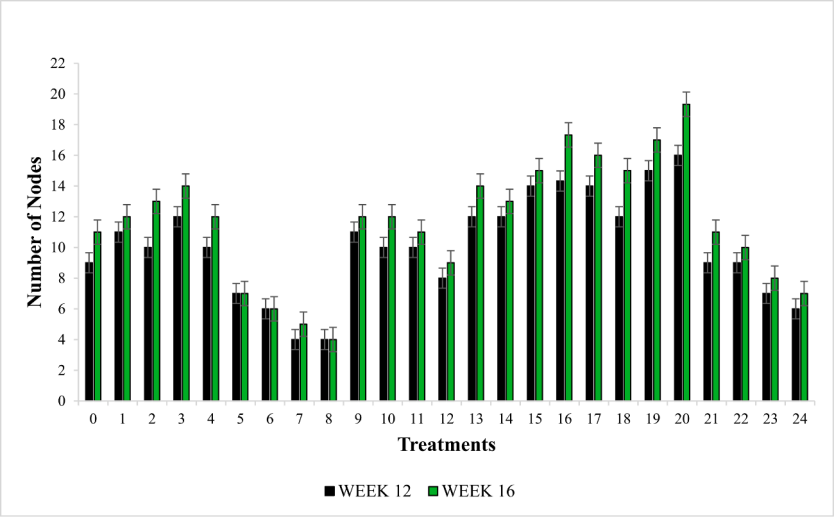

Fig. 18. Week 12th and 16th number of nodes of tomato plants subjected to ZnO NPs and salt stress.

plant concentration, salt, pH, and temperature. The optimum synthesis conditions are analyzed using RSM. Multiple factors can affect the response of a system, and the interaction between these factors can be analyzed (Es-Haghi et al., 2021). Equations. 2 and 3 indicated that *P. karka* positively affected the biogenic synthesis of ZnO NPs. This revealed that *P. karka* plant plays a vital role in synthesizing Zn^{+2} to Zn^{0}**.** This leads to the interaction of secondary metabolites in *P. karka* with a reducing agent and increases the synthesis of ZnO NPs. The presence of secondary metabolites enhances the reduction capacity of biomolecules involved in the reduction process, as reported by Hoseinpour et al. (2017). The results showed that run number 21 gave the highest absorbance of ZnO NPs synthesized from *P. karka* with 5 gm of plant leaf powder, 1 g of salt having 6.5 pH at 37.5 °C of temperature. The maximum absorbance was 0.699 a.u.

Synthesis of nanoparticles using halophytes such as *P. karka* contains a broad range of applications in agriculture, the food industry, and many others due to enriching sources of metabolites such as proteins, vitamins, coenzymes, phenols, flavonoids, and carbohydrates (Munir et al., 2021; Hanif et al., 2023). The halophytic metabolites react with the metal ions and reduce their size to nano-range. The flavonoid contains multiple functional groups along with the –OH group. It is considered that the –OH group of flavonoids is responsible for the reduction of metal ions into NPs (Naseer et al., 2020). The UV–Vis analysis of ZnO NPs synthesized from *P. karka* showed the highest absorbance at 331 nm and leaves extract absorbance at 302 nm. The same results are reported by Faisal et al. (2021). The addition of zinc acetate dihydrate solution in leaf extract of halophyte may cause the physio-chemical changes in aqueous solution. In the current study, the change of color from light green to pale yellow indicated the formation of ZnO NPs from the leaf extract of *P. karka* (Naseer et al., 2020).

FTIR was used to identify the possible functional groups present in the capping proteins associated with synthesized ZnO nanoparticles. These functional groups are considered to be responsible for the reduction and stabilization of ZnO NPs. The FTIR spectra of leaf extract showed a peak at 3770.83 cm^{-1}, which shifted to 3832.57 cm^{-1} when reacted with Zinc acetate dihydrate to form ZnO

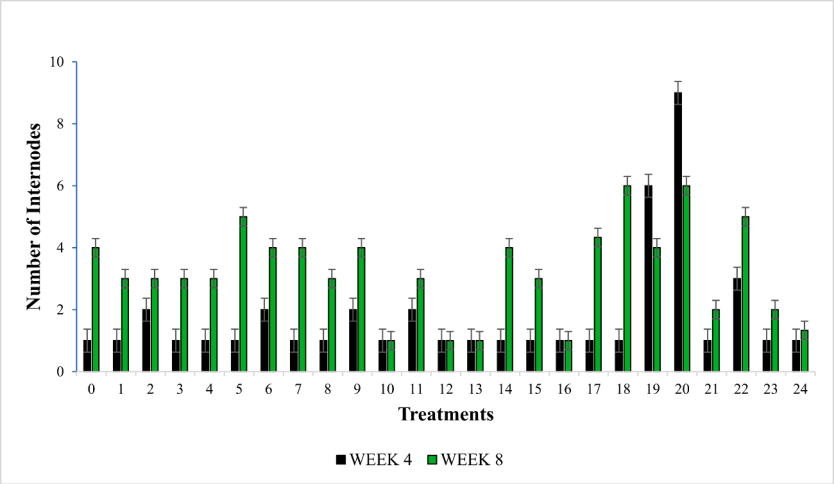

Fig. 19. Week 4th and 8th number of internodes of tomato plants subjected to ZnO NPs and salt stress.

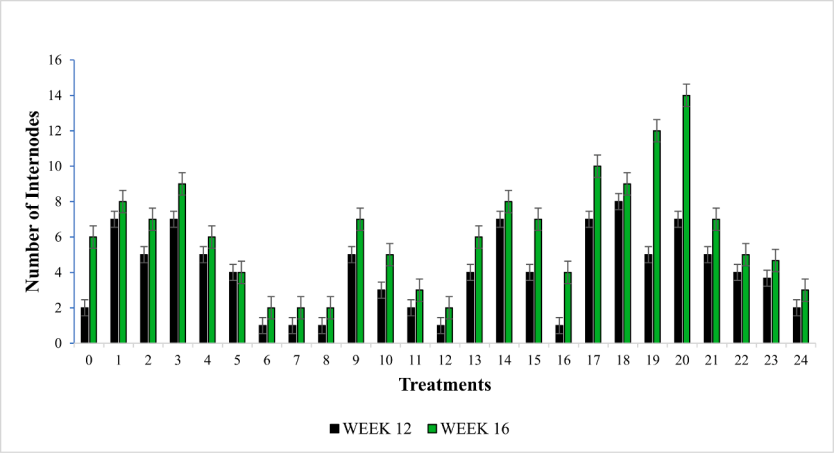

Fig. 20. Week 12th and 16th number of internodes of tomato plants subjected to ZnO NPs and salt stress.

Fig. 21. Ex vitro experimental setup of tomato plants subjected to ZnO NPs and salt stress.

NPs. This change in peak occurs due to the broad stretching vibration of the hydroxyl group (OH), which also corresponds to the protein N–H amide present in the leaves extract. The reason behind this phenomenon is the interaction of plant protein and nanoparticles, which occurs through the free amine group or cysteine residues present in plant proteins (Al-Kordy et al., 2021). The same results were reported by Goutam et al. (2017) who also observed the OH stretching of the hydroxyl group. The peak observed at 661.58 cm^{-1} in leaves extract of *P. karka,* showed that the presence of functional groups, saponins and phenolic compounds in leaf extract indicated that extract has a potential to act as a capping agent. The shifting of some peaks from leaves extract to ZnO NPs spectra confirmed the reduction of Zn^{+2} to Zn^{0} as reported by Naseer et al. (2020), who also stated that functional groups such as OH group

Fig. 22. Morphological traits of tomato plants subjected to ZnO NPs under salt stress a) Shoot length b) Number of leaves c) Number of nodes d) Number of internodes.

plays a significant role in the bioreduction of salt and capping of ZnO NPs. Somehow, the results showed that the capping proteins in leaf extracts aid in the stabilization of metallic nanoparticles, which in return prevents the agglomeration of nanoparticles.

The XRD pattern of biosynthesized ZnO NPs from *P. karka* revealed the high-intensity, well-defined peaks indicating the synthesis of the nanocrystalline phase. The result showed that the average crystal size of synthesized ZnO NPs decreases as the concentration of plant extract increases. The reason was that the high amount of plant extract used during the synthesis process leads to the effective capping and stabilizing of synthesized nanoparticles. These results have also been reported in previous studies related to the green synthesis of Zinc oxide nanoparticles (Mathubala, 2012). The SEM results indicated that the size and shape of synthesized nanoparticles vary due to the use of zinc acetate dihydrate, which acts as a precursor. Zinc acetate dihydrate lets the zinc oxide molecules grow gradually; as a result, it forms small spherical structures. The kinds of observations are reported by Alamdari et al. (2020). The high positive potential value of ZnO NPs synthesized from *P. karka* indicates that these biogenically synthesized nanoparticles are highly stable. The presence of electrostatic repulsive forces prevents the agglomeration between nanoparticles. Generally, the zeta potential value between (+ 30 mV to – 30 mV) indicates the good stability of nanoparticles. It was clear from the results that the size of synthesized particles was less than 100 nm in diameter. The same results are reported by Faisal et al. (2021) which states that the ZnO NPs synthesized from *Myristica fragrans* also showed the size and potential of nanoparticles less than 100 nm. The presence of multiple functional groups present in the halophytic extract has been absorbed on the surface of synthesized ZnO NPs, which may affect its zeta potential. There is a direct relationship between the absorption of halophytic secondary metabolites and zeta potential.

A study suggests that the variability in resistance to salinity depends upon the plant species (Ashraf and Foolad, 2007). The enhanced growth of tomato plants under different salt concentrations can be used as an indicator that ZnO NPs are a good source for tomato plants. Our findings indicated that plants under treatments T5 (10 mM NaCl), T6 (20 mM NaCl), T7 (50 mM NaCl), and T8 (100 mM NaCl) caused the decrease in plant shoot length, number of leaves, number of nodes as well internodes. Thus, it can be con-

cluded that as the salinity levels increase, the tomato plant growth parameters decrease. Our results were similar to Rahman et al. (2018), who stated that the growth parameters of tomato plants were negatively affected by 6–8 ds/m salinity stress. Tomato plants growing under salinity stress in early developmental stages may negatively affect crop production (Siddiky et al., 2015). The reason behind the decreased growth in tomato plants under salinity stress is the ionic imbalance in plants due to the excess amount of salt. It has been observed that under salt stress, the uptake of Na^+ ions increased as compared to K^+ and Ca^+, leading to ionic deficiencies (Shoukat et al., 2020). Salinity is a crucial abiotic factor that limits the growth and development of tomato plants (Guo et al., 2022; Abideen et al., 2014).

Zinc is a beneficial element for plants; thus, it can have a positive effect when applied as nanoparticles. ZnO NPs have shown stimulating effects on tomato plants under salt stress (Ahmed et al., 2023). In the present study, the study of growth parameters reveals that they increase significantly when exposed to ZnO NPs under salt stress. Our results stated that plant growth parameters showed the best growth at 50 mgL^{-1} ZnO NPs. The same results were reported by Quiterio-Gutierrez et al. (2019), who also concluded that 50 ppm of ZnO NPs showed an enhanced shoot length in tomato plants. In the present study, tomato plants were exposed to multiple concentrations of ZnO NPs (10 mgL^{-1}, 20 mgL^{-1}, 50 mgL^{-1}, and 100 mgL^{-1}) under salt stress (10 mM NaCl, 20 mM NaCl, 50 mM NaCl, and 100 mM NaCl). The results concluded that plants treated with 10 mgL^{-1}, 20 $mgL^{-1,}$ and 50 mgL^{-1} of ZnO NPs improved growth criteria, while plants treated with 100 mgL^{-1} led to decreased growth parameters of stressed plants. Similar to our findings, Al-Antary et al. (2020) reported that 50 ppm of ZnO NPs increased the broad bean growth under salt stress. The increased concentration of ZnO NPs (100 mgL^{-1}) causes the toxicity in plant nucleic acid and cell division. This claim was supported by the study reported by López-Moreno et al. (2010), who observed the phytotoxicity on soybean plants by the high concentration of ZnO NPs. Another research reported that increased concentration of ZnO NPs caused a negative impact on *Brassica nigra* root and shoot length (Zafar et al., 2016).

The current research analyzed the effect of foliar application of ZnO NPs on tomato plant under salinity stress on plant growth parameters. The results demonstrated that 50 and 20 mgL^{-1} of ZnO NPs showed increased plant growth parameters under 50 and 100 mM NaCl. In agreement with our results, Ragab et al. (2022) also reported that ZnO NPs treated faba bean plants boosted their growth and yield under salt stress. The foliar application of ZnO NPs may assist in reducing the salt stress on plant cells, causing an increase in shoot length, number of leaves, and other morphological traits. It was observed that NPs always have a positive effect on multiple morphological aspects of plants as they produce enhanced root and shoot growth in horticulture crops (Khalid et al., 2022). The foliar application of ZnO NPs on tomato plants enhanced the shoot length, number of leaves, nodes and the intermodal length even at 100 mM of NaCl.

This was due to the presence of ZnO NPs serving to reduce the sodium toxicity and concomitantly increasing the by-product metabolism and photosynthetic activity. In addition, ZnO NPs could enter the cell walls and increasing the levels of auxin (IAA) which helps to promote cell division (in the presence of cytokinins), cell elongation and mineral absorption. Recently, Zhang et al. (2022) demonstrated that tomato plants were able to attain better growth while undergoing salinity stress by the foliar application of ZnO NPs (Zhang et al., 2022).

5. Conclusion

In the present study, ZnO NPs were synthesized using foliar extracts of *P. karka.* Zinc acetate dihydrate was used as a precursor. Halophytic leaf extract was used as a stabilizing and reducing agent. RSM was used to optimize the process of nanoparticle synthesis. The RSM experimental setup showed that pH and plant are significant factors in synthesizing ZnO NPs. UV–Vis spectrum of ZnO NPs by *P. karka* showed a distinct peak at 331 nm. Furthermore, the synthesis of nanoparticles was confirmed by FTIR technique, which clearly showed the production of ZnO NPs; also revealed that the plant extract contains phytochemicals that could serve as a capping and stabilizing agent. The spectra obtained by XRD analysis showed that the synthesized nanoparticles are of crystalline structure. Meanwhile, SEM and DLS analyses defined the sizes of synthesized ZnO NPs from *P. karka.* The tomato growth experiment demonstrated that the physiological effects of high salt stress were reduced by using ZnO NPs. It was plausible that the optimum concentration of ZnO NPs improved the levels of plant secondary metabolites and osmolytes which resulted in the enhanced plant growth parameters. Conversely, either in the presence or absence of salt stress, a high concentration of ZnO NPs appeared to cause symptoms of phytotoxicity in the plants. This research revealed that zinc can assist in maintaining the structure of plasma membrane while undergoing extreme salinity stress; plausibly by maintaining the entry of sodium ions into plant cells thereby reducing the effects of oxidative stress.

CRediT authorship contribution statement

Maria Hanif: Conceptualization, Data curation, Formal analysis, Writing – original draft, Writing – review & editing. **Neelma Munir:** Conceptualization, Data curation, Formal analysis, Supervision, Validation, Writing – original draft, Writing – review & editing. **Zainul Abideen:** Methodology, Supervision, Writing – review & editing. **Jean Wan Hong Yong:** Funding acquisition, Writing – original draft, Writing – review & editing. **Ali El-Keblawy:** Writing – review & editing, Data curation, Writing – original draft. **Mohamed A. El-Sheikh:** Funding acquisition, Supervision, Writing – review & editing.

Declaration of competing interest

The authors declare that they have no known competing financial interests or personal relationships that could have appeared to influence the work reported in this paper.

Data availability

Data will be made available on request.

Acknowledgements

The authors would like to extend their sincere appreciation to the Researchers Supporting Project Number (RSP 2023R182) King Saud University, Riyadh, Saudi Arabia. This study was conducted under the supports of Project #: 20-17444/NRPU/R&D/HEC/2021 funded by "Higher Education Commission (HEC) Pakistan.

References

Abideen, Z., Koyro, H.W., Huchzermeyer, B., Ahmed, M.Z., Gul, B., Khan, M.A., 2014. Moderate salinity stimulates growth and photosynthesis of *Phragmites karka* by water relations and tissue specific ion regulation. Environ. Exp. Bot. 105, 70–76.

Ahmed, M., Decsi, K., Tóth, Z., 2023. Different tactics of synthesized zinc oxide nanoparticles, homeostasis ions, and phytohormones as regulators and adaptatively parameters to alleviate the adverse effects of salinity stress on plants. Life 13, 73.

Al Jabri, H., Saleem, M.H., Rizwan, M., Hussain, I., Usman, K., Alsafran, M., 2022. Zinc oxide nanoparticles and their biosynthesis: overview. Life 12, 594.

Al-Antary, T.A., Kahlel, A., Ghidan, A., Asoufi, H., 2020. Effects of nanotechnology liquid fertilizers on fruit set and pods of broad bean (*Vicia faba* L.). Fresenius Environ. Bull. 29, 4794–4798.

Al-Kordy, H.M., Sabry, S.A., Mabrouk, M.E., 2021. Statistical optimization of experimental parameters for extracellular synthesis of zinc oxide nanoparticles by a novel haloalaliphilic *Alkalibacillus* sp. W7. Sci. Rep. 11, 10924.

Alamdari, S., Sasani, G.M., Lee, C., Han, W., Park, H.H., Tafreshi, M.J., Afarideh, H., Ara, M.H.M., 2020. Preparation and characterization of zinc oxide nanoparticles using leaf extract of *Sambucus ebulus*. Appl. Sci. 10, 3620.

Alharby, H.F., Metwali, E.M., Fuller, M.P., Aldhebiani, A.Y., 2017. Impact of application of zinc oxide nanoparticles on callus induction, plant regeneration, element content and antioxidant enzyme activity in tomato (*Solanum lycopersicum* Mill) under salt stress. Arch. Biol. Sci. 68, 723–735.

Ali, S., Mehmood, A., Khan, N., 2021. Uptake, translocation, and consequences of nanomaterials on plant growth and stress adaptation. J. Nanomater. 2021, 1–17.

Ansari, I., Ejaz, U., Abideen, Z., Gulzar, S., Syed, M.N., Liu, J., Li, W., Fu, P., Sohail, M., 2021. Wild halophytic *Phragmites karka* biomass saccharification by bacterial enzyme cocktail. Front. Microbiol. 12, 714940.

Ashraf, M.F.M.R., Foolad, M.R., 2007. Roles of glycine betaine and proline in improving plant abiotic stress resistance. Environ. Exp. Bot. 59, 206–216.

Bora, K.A., Hashmi, S., Zulfiqar, F., Abideen, Z., Ali, H., Siddiqui, Z.S., Siddique, K.H., 2022. Recent progress in bio-mediated synthesis and applications of engineered nanomaterials for sustainable agriculture. Front. Plant Sci. 13, 999505.

Chan, S.S., Low, S.S., Chew, K.W., Ling, T.C., Rinklebe, J., Juan, J.C., Ng, E.P., Show, P.L., 2022. Prospects and environmental sustainability of phyconanotechnology: a review on algae-mediated metal nanoparticles synthesis and mechanism. Environ. Res. 212, 13140.

Es-Haghi, A., Taghavizadeh, Y.M.E., Sharifalhoseini, M., Baghani, M., Yousefi, E., Rahdar, A., Baino, F., 2021. Application of response surface methodology for optimizing the therapeutic activity of ZnO nanoparticles biosynthesized from *Aspergillus niger*. Biomimetics 6, 34.

Faisal, S., Jan, H., Shah, S.A., Shah, S., Khan, A., Akbar, M.T., Rizwan, M., Jan, F., Wajidullah, Akhtar, N., Khattak, A., 2021. Green synthesis of zinc oxide (ZnO) nanoparticles using aqueous fruit extracts of *Myristica fragrans*: their characterizations and biological and environmental applications. ACS Omega 6, 9709–9722.

Goutam, S.P., Yadav, A.K., Das, A.J., 2017. Coriander extract mediated green synthesis of zinc oxide nanoparticles and their structural, optical and antibacterial properties. J. Nanosci. Technol. 249–252.

Guo, M., Wang, X.S., Guo, H.D., Bai, S.Y., Khan, A., Wang, X.M., Gao, Y.M., Li, J.S., 2022. Tomato salt tolerance mechanisms and their potential applications for fighting salinity: a review. Front. Plant Sci. 13, 949541.

Hanif, M., Munir, N., Abideen, Z., Dias, D.A., Hessini, K., El-Keblawy, A., 2023. Enhancing tomato plant growth in a saline environment through the eco-friendly synthesis and optimization of nanoparticles derived from halophytic sources. Environ. Sci. Pollut. Res. 1–25. https://doi.org/10.1007/s11356-023-30626-1.

Hoseinpour, V., Souri, M., Ghaemi, N., Shakeri, A., 2017. Optimization of green synthesis of ZnO nanoparticles by *Dittrichia graveolens* (L.) aqueous extract. Health Biotechnol. Biopharm. 1, 39–49.

Hosny, M., Fawzy, M., El-Borady, O.M., Mahmoud, A.E.D., 2021. Comparative study between *Phragmites australis* root and rhizome extracts for mediating gold nanoparticles synthesis and their medical and environmental applications. Adv. Powder Technol. 32, 2268–2279.

Huang, B., Chen, F., Shen, Y., Qian, K., Wang, Y., Sun, C., Cui, H., 2018. Advances in targeted pesticides with environmentally responsive controlled release by nanotechnology. Nanomaterials 8 (2), 102.

Jakhar, A.M., Aziz, I., Kaleri, A.R., Hasnain, M., Haider, G., Ma, J., Abideen, Z., 2022. Nano-fertilizers: a sustainable technology for improving crop nutrition and food security. NanoImpact 100411.

Kesawat, M.S., Satheesh, N., Kherawat, B.S., Kumar, A., Kim, H.U., Chung, S.M., Kumar, M., 2023. Regulation of reactive oxygen species during salt stress in plants and their crosstalk with other signaling molecules—current perspectives and future directions. Plants 12, 864.

Khalid, M.F., Iqbal, K.R., Jawaid, M.Z., Shafqat, W., Hussain, S., Ahmed, T., Rizwan, M., Ercisli, S., Pop, O.L., Alina, M.R., 2022. Nanoparticles: the plant saviour under abiotic stresses. Nanomaterials 12, 3915.

López-Moreno, M.L., de la Rosa, G., Hernández-Viezcas, J.Á., Castillo-Michel, H., Botez, C.E., Peralta-Videa, J.R., Gardea-Torresdey, J.L., 2010. Evidence of the differential biotransformation and genotoxicity of ZnO and CeO_2 nanoparticles on soybean (*Glycine max*) plants. Environ. Sci. Technol. 44, 7315–7320.

Ma, Y., Dias, M.C., Freitas, H., 2020. Drought and salinity stress responses and microbe-induced tolerance in plants. Front. Plant Sci. 11, 591911.

Mathubala, K.A.G., 2012. Synthesis and characterization of zinc oxide nanoparticle using *Chenopodium album* as a biotemplate and its larvicidal activity evaluation. 11, 1222–1235.

Meng, X., Zhou, J., Sui, N., 2018. Mechanisms of salt tolerance in halophytes: current understanding and recent advances. Open Life Sci. 13, 149–154.

Munir, N., Hanif, M., Dias, D.A., Abideen, Z., 2021. The role of halophytic nanoparticles towards the remediation of degraded and saline agricultural lands. Environ. Sci. Pollut. Res. 28, 1–23.

Naseer, M., Aslam, U., Khalid, B., Chen, B., 2020. Green route to synthesize Zinc Oxide Nanoparticles using leaf extracts of *Cassia fistula* and *Melia azadarach* and their antibacterial potential. Sci. Rep. 10, 9055.

Qasim, M., Abideen, Z., Adnan, M.Y., Gulzar, S., Gul, B., Rasheed, M., Khan, M.A., 2017. Antioxidant properties, phenolic composition, bioactive compounds and nutritive value of medicinal halophytes commonly used as herbal teas. South Afr. J. Bot. 110, 240–250.

Ragab, S.M., Turoop, L., Runo, S., Nyanjom, S., 2022. Nanoparticle treatments based on zinc oxide and *Moringa oleifera* leaf extracts alleviate salinity stress in faba bean (*Vicia faba* L.). J. Agric. Chem. Environ. 11, 42–65.

Rahman, M.M., Hossain, M., Hossain, K.F.B., Sikder, M.T., Shammi, M., Rasheduzzaman, M., Hossain, M.A., Alam, A.M., Uddin, M.K., 2018. Effects of NaCl-salinity on tomato (*Lycopersicon esculentum* Mill.) plants in a pot experiment. Open Agric. 3, 578–585.

Shafey, A.M.E., 2020. Green synthesis of metal and metal oxide nanoparticles from plant leaf extracts and their applications: a review. Green Process. Synth. 9, 304–339.

Shang, Y., Hasan, M.K., Ahammed, G.J., Li, M., Yin, H., Zhou, J., 2019. Applications of nanotechnology in plant growth and crop protection: a review. Molecules 24, 2558.

Shoukat, E., Ahmed, M.Z., Abideen, Z., Azeem, M., Ibrahim, M., Gul, B., Khan, M.A., 2020. Short and long term salinity induced differences in growth and tissue specific ion regulation of *Phragmites karka*. Flora 263, 151550.

Siddiky, M.A., Khan, M.S., Rahman, M.M., Uddin, M.K., 2015. Performance of tomato (*Lycopersicon esculentum* Mill.) germplasm to salinity stress. Bangladesh J. Bot. 44,

193–200.
Tao, Y., Wu, P., Dai, Y., Luo, X., Manickam, S., Li, D., Han, Y., Show, P.L., 2022. Bridge between mass transfer behavior and properties of bubbles under two-stage ultrasound-assisted physisorption of polyphenols using macroporous resin. J. Chem. Eng. 436, 135158.
Ying, S., Guan, Z., Ofoegbu, P.C., Clubb, P., Rico, C., He, F., Hong, J., 2022. Green synthesis of nanoparticles: current developments and limitations. Environ. Technol. Innov. 26, 102336.
Zafar, H., Ali, A., Ali, J.S., Haq, I.U., Zia, M., 2016. Effect of ZnO nanoparticles on *Brassica nigra* seedlings and stem explants: growth dynamics and antioxidative response. Front. Plant Sci. 7, 535.
Zhang, H., Sun, X., Dai, M., 2022. Improving crop drought resistance with plant growth regulators and rhizobacteria: mechanisms, applications, and perspectives. Plant Commun. 3, 1–15.